

Performance analysis of single-focus phase singularity based on elliptical reflective annulus quadrangle-element coded spiral zone plates

Huaping Zang(臧华平), Baozhen Wang(王宝珍), Chenglong Zheng(郑程龙), Lai Wei(魏来), Quanping Fan(范全平), Shaoyi Wang(王少义), Zuhua Yang(杨祖华), Weimin Zhou(周维民), Leifeng Cao(曹磊峰), and Haizhong Guo(郭海中)

Citation: Chin. Phys. B, 2024, 33 (**1**): 014209. DOI: 10.1088/1674-1056/acde4f
Journal homepage: http://cpb.iphy.ac.cn; http://iopscience.iop.org/cpb

What follows is a list of articles you may be interested in

Young's double slit interference with vortex source

Qilin Duan(段琦琳), Pengfei Zhao(赵鹏飞), Yuhang Yin(殷玉杭), and Huanyang Chen(陈焕阳)
Chin. Phys. B, 2024, 33 (**1**): 014202. DOI: 10.1088/1674-1056/acfdfd

Multi-channel generation of vortex beams with controllable polarization states and orbital angular momentum

Ziyao Lyu(吕子瑶), Pan Wang(王潘), and Changshun Wang(王长顺)
Chin. Phys. B, 2023, 32 (**12**): 124209. DOI: 10.1088/1674-1056/ace767

Optical chirality induced by spin-orbit interaction of light in a tightly focused Laguerre-Gaussian beam

Mingchao Zhu(朱明超), Shenggui Fu(付圣贵), and Zhongsheng Man(满忠胜)
Chin. Phys. B, 2023, 32 (**11**): 114202. DOI: 10.1088/1674-1056/acefc9

A crossed focused vortex beam with application to cold molecules

Meng Xia(夏梦), Yaling Yin(尹亚玲), Chunying Pei(裴春莹), Yuer Ye(叶玉儿), Ruoxi Gu(顾若溪), Kang Yan(严康), Di Wu(吴迪), Yong Xia(夏勇), and Jianping Yin(印建平)
Chin. Phys. B, 2021, 30 (**11**): 114202. DOI: 10.1088/1674-1056/abf915

Three-Airy autofocusing beams

Xiao-Hong Zhang(张小红), Fei-Li Wang(王飞利), Lu-Yang Bai(白露阳), Ci-Bo Lou(楼慈波), Yi Liang(梁毅)
Chin. Phys. B, 2020, 29 (**6**): 064204. DOI: 10.1088/1674-1056/ab84d2

Performance analysis of single-focus phase singularity based on elliptical reflective annulus quadrangle-element coded spiral zone plates

Huaping Zang(臧华平)[1], Baozhen Wang(王宝珍)[1], Chenglong Zheng(郑程龙)[1], Lai Wei(魏来)[2], Quanping Fan(范全平)[2], Shaoyi Wang(王少义)[2], Zuhua Yang(杨祖华)[2,‡], Weimin Zhou(周维民)[2], Leifeng Cao(曹磊峰)[3], and Haizhong Guo(郭海中)[1,†]

[1] *Key Laboratory of Material Physics, Ministry of Education, School of Physics and Microelectronics, Zhengzhou University, Zhengzhou* 450052, *China*
[2] *National Key Laboratory for Laser Fusion, Research Center of Laser Fusion, China Academy of Engineering Physics, Mianyang* 621900, *China*
[3] *School of Engineering Physics, Shenzhen Technology University, Shenzhen* 518118, *China*

(Received 19 April 2023; revised manuscript received 28 May 2023; accepted manuscript online 14 June 2023)

Optical vortices generated by the conventional vortex lens are usually disturbed by the undesired higher-order foci, which may lead to additional artifacts and thus degrade the contrast sensitivity. In this work, we propose an efficient methodology to combine the merit of elliptical reflective zone plates (ERZPs) and the advantage of spiral zone plates (SZPs) in establishing a specific single optical element, termed elliptical reflective annulus quadrangle-element coded spiral zone plates (ERAQSZPs) to generate single-focus phase singularity. Differing from the abrupt reflectance of the ERZPs, a series of randomly distributed nanometer apertures are adopted to realize the sinusoidal reflectance. Typically, according to our physical design, the ERAQSZPs are fabricated on a bulk substrate; therefore, the new idea can significantly reduce the difficulty in the fabrication process. Based on the Kirchhoff diffraction theory and convolution theorem, the focusing performance of ERAQSZPs is calculated. The results reveal that apart from the capability of generating optical vortices, ERAQSZPs can also integrate the function of focusing, energy selection, higher-order foci elimination, as well as high spectral resolution together. In addition, the focusing properties can be further improved by appropriately adjusting the parameters, such as zone number and the size of the consisted primitives. These findings are expected to direct a new direction toward improving the performance of optical capture, x-ray fluorescence spectra, and forbidden transition.

Keywords: optical vortex, single-focus, spiral zone plate, topological charges

PACS: 42.79.Ci, 42.25.Fx, 07.85.Fv **DOI:** 10.1088/1674-1056/acde4f

1. Introduction

Optical vortices (OVs) are known to be singular phase structures that carry orbital angular momentum (OAM).[1,2] Considering the consequently unique inherent properties, such as zero on-axis intensity and Poynting vector spirals,[3] their application is an important research topic for particle trapping and manipulation,[4,5] optical information coding and transmission,[6,7] phase-contrast microscopy[8,9] and stimulated emission depletion microscopy.[10] Specifically, OVs retain an angle-dependent spiral phase called $\Phi = P\varphi$, where P is the topological charge (TC), φ represents the azimuth angle.[11–13] Various effective methods, such as computer holography,[14] spiral phase plate (SPP),[15] spiral zone plates (SZPs),[16–18] metasurface,[19] spatial light modulators (SLM),[20] spiral photon sieves (SPS),[21] have been investigated and adopted to generate OVs.

In recent years, the OVs with helical phase beams from extreme ultraviolet to x-ray region have attracted the particular attention of physicists by extending microscopic and spectral applications to atomic or nanoscale.[22] The torque generated by the OAM beams can provide additional degrees of freedom to the interaction between light and matter,[1] and make important progress in the study of dynamic detection of chiral systems,[23] coherent symmetry and stack diffraction imaging,[24] and the dichroism induced by OAM.[25] An accessible way to create extreme ultraviolet and x-ray beams carrying OAM is to develop the nonlinear process of high-harmonic generation,[26] guaranteeing important practical application prospects for the study of forbidden transitions in atomic and molecular physics and high-energy density physics.[27] Nevertheless, previous theoretical and experimental results both reveal that the topological charges (TCs) of high-harmonic vortices are usually uncontrollable and increase with harmonic order.[28,29]

In particular, the SZPs, which combine the radial Hilbert transform filtering operation with the Fresnel zone plates (FZPs) focusing operation, provide an efficient methodology for producing helical beams with OAM considering their outstanding characteristics of compact size, light weight, and degree of design flexibility.[30] According to the typical princi-

†Corresponding author. E-mail: hguo@zzu.edu.cn
‡Corresponding author. E-mail: yangzuhua@caep.cn

© 2024 Chinese Physical Society and IOP Publishing Ltd

ple, arbitrary amount of OAM can also be imparted on any harmonic beam. However, due to the fabrication reasons and volume diffraction effects, the spatial resolution of the conventional transmissive focusing devices such as FZPs and SZPs cannot be less than 10 nm.[31,32] The subsequently proposed elliptical reflection zone plates (ERZPs) have overcome these shortcomings with high resolution, and are an optimum and important breakthrough to monochromatic and the low energy band of the ultrafast betatron radiation.[33]

Despite all this, the ERZPs and SZPs both exhibit the characteristic as multifocal lenses, and therefore the spectrum of which will be contaminated by the unavoidable higher foci. In addition, the diffraction efficiency will be reduced and additional artifacts will be introduced, limiting their extensive applications in ultra-high precision x-ray or extreme ultraviolet spectral analysis technology.[34,35] To alleviate such spurious effects originating from the higher-order foci induced by the inherent binary nature of diffraction optical elements (DOEs), Gabor zone plates (GZPs) and improved GZPs were proposed to eliminate the interference of higher-order foci with an ideal sinusoidal transmittance between the transparent and opaque zones.[36–43]

Enlightened by these proposals, in this work we present a new strategy to combine the merit of ERZPs and the advantage of SZPs in establishing a specific single optical element, termed elliptical reflective annulus quadrangle-element coded spiral zone plates (ERAQSZPs). According to our physical design, a series of randomly distributed annulus quadrangle-shaped nanometer structure apertures are adopted to replace the abrupt structures of the ERZPs to realize the desired sinusoidal reflectance. Based on the Kirchhoff diffraction theory and convolution theorem,[44] the focusing performance of such optics has been analyzed theoretically and numerically. Relative to the multi-foci irradiance generated by the ERZPs, on the one hand, the new idea can generate OVs with controllable OAM, and on the other hand can suppress the unavoidable higher-order foci with a purity and high-resolution spectrum. Such a device performs as an ideal GZP. However, the continuous surface was refined by simple binary structures. Moreover, it is known that the reflective device is fabricated on a bulk substrate and it adopts the grazing incidence mode. Hence, to obtain the same focus size, the width of the outmost zone is larger than that of the transmissive one and the difficulty in fabrication will be reduced. In addition, the focusing properties can be further improved by appropriately adjusting the parameters, such as zone number and the size of the consisted primitives. The present findings are expected to open a new avenue toward improving the performance of optical capture,[45] x-ray fluorescence spectra,[46,47] and forbidden transition.[48]

2. Design and method

In this paper, we start with the physical design of elliptical reflective spiral zone plates (ERSZPs), as shown in Fig. 1(b), and combine the merits of ERZPs, as shown in Fig. 1(a), with the advantages of SZPs to preserve the capability to produce OVs and disperse different incident energies with larger dimensions. Consequently, the reflectance of the ERSZPs can be represented as follows:

$$\left[z_n + \frac{N\lambda\cos\theta}{2\nu\sin^2\theta}\right] + \frac{x_n}{\sin^2\theta} = \frac{N\lambda f}{\sin^2\theta}, \tag{1}$$

where $\nu = (R_1/R_2+1)/(R_1/R_2-1)$, $N = -P\phi/\pi + 2(n-1)$, R_1 and R_2 are the object distance and image distance, respectively. Here f is the focal length, θ is the grazing incidence angle, λ is the designed central wavelength, P and ϕ represent the TCs and the azimuth, respectively.

Nevertheless, the binary reflectance, which takes on the values of 0 and 1 between the adjacent transparent and opaque grooves for a conventional ERZPs, will lead to the interference of higher foci. To obtain the desired single-focus characteristics as that of the ideal GZPs, we further complete the design of proposed ERAQSZPs by appropriately arranging a large number of annulus quadrangle-shaped structure primitives instead of the abrupt reflections to construct a reflective single-focus optical element.

Specifically, we divide the annular ring of the ERSZPs into M primitives on average. These closely connected primitives form an elliptical ring band, and the field angle of the primitives is approximately $2\pi/M$. The radial size of each primitive is half of the width of the elliptical band, so the radial size of the primitives with different bands is different. Then, the size of the primitive should be appropriately selected and optimized to achieve the sinusoidal reflectivity of the device without increasing the computational difficulty. Significantly, given that ERZPs can be seen as the superposition of the meridional and the sagittal direction gratings, the typical proposed ERAQSZPs have also been endowed with two focusing directions, i.e., the sagittal and meridional directions. Meanwhile, the meridional direction determines the spectral and the focusing resolutions in the spectral direction, while the sagittal direction determines the spatial resolution, which can reach sub-nanometer in the spatial direction of the detector plane. Hence, if the incident beams include different wavelengths modulated by ERAQSZPs, then the generated OVs can be dispersed and focused on different positions along the optical axis without the interference of the higher foci.

In detail, the expression of the ERAQSZPs with excellent single-focus focusing performance can be represented as follows:

$$\left[z_n + \frac{N\lambda\cos\theta}{2\nu\sin^2\theta}\right] + \frac{x_n}{\sin^2\theta} = \frac{N-(\mathrm{rand}-0.5)\cdot\lambda f}{\sin^2\theta}. \tag{2}$$

The parameters in Eq. (2) have the same representations as those in Eq. (1). According to our physical design, the alternative transparent and opaque zones have been substituted by lots of staggered annulus quadrangle nanometer apertures to realize the desired sinusoidal reflectance. Therefore, we introduce a random item whose value varies from 0 to 1 in Eq. (2) to control the positions and arrangement of the consisted primitives. The structure of ERAQSZPs is presented in Fig. 1(c).

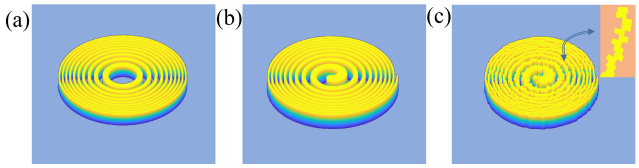


Fig. 1. (a) Schematic view of ERZPs. (b) Schematic view of ERSZPs. (c) Schematic view of ERAQSZPs with annular quadrilateral-elements. The illustration is a partial element enlarged view.

Generally, in the diffraction process of ERAQSZPs, the incident beam is a grazing incidence, as illustrated in Fig. 2(a), which can dramatically reduce the requirements for the effective size of the outmost ring, as well as the fabrication difficulty. In addition, to clearly identify the single-order focusing performance of the ERAQSZPs, we present a comparison of integral curves of reflectance of ERAQSZPs and the ERSZPs in Fig. 2(b). Consequently, by comparing with the binarization reflectance of ERSZPs, we can readily deduce that the reflectance of ERAQSZPs can realize an approximately sinusoidal variation such as that of the ideal Gabor zone spiral plates (GSZPs), indicating that it is an effective monochromator for incident irradiation in the generation of phase singularity.

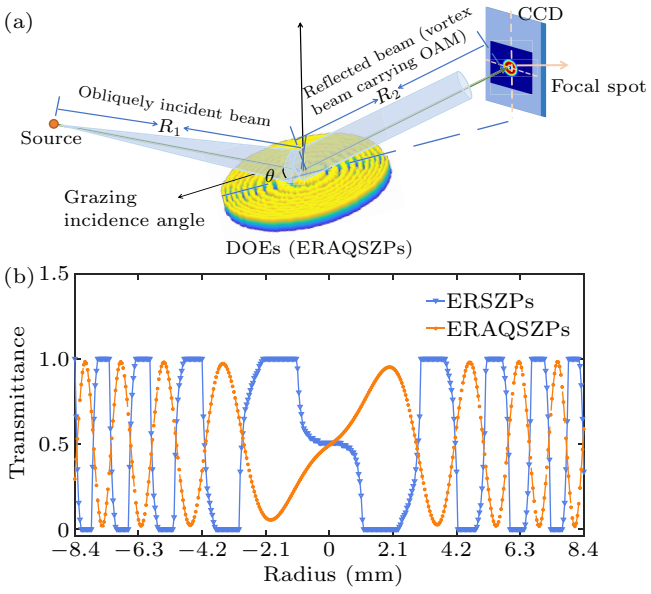


Fig. 2. (a) Focusing principle diagram of ERAQSZPs. (b) Comparison of reflectivity function distribution curves between ERSZPs (blue) and ERAQSZPs (yellow).

3. Numerical results and discussion

To evaluate the advantages of the proposed physical design, based on the Kirchhoff diffraction theory and convolution theorem, the focusing performance of the ERAQSZPs was analyzed. As we mentioned above, the nonlinear process of high-harmonic generation (HHG) is an effective method to generate extreme ultraviolet and x-ray OVs. Hence, in our calculation, we select the 19-order incident energy (29.83 eV) of HHG with 1.57 eV center energy generated by infrared laser and rare gas Ar to carry out the corresponding verification. In particular, to obtain symmetrical circular profile single-focus OVs, the ratio of the length of the meridional direction and sagittal direction of the ERAQSZPs has a certain restriction and should be appropriately chosen. In this simulation, the values of the meridian length and the sagittal length have been, respectively, adopted as 42 mm and 3.2 mm, and it can be further optimized to achieve a better phase structure. The object and image distances are 0.75 m and 1.5 m, respectively. In addition, to satisfy the requirements of total reflection of metal materials, the grazing incidence angle is set to 4°. The specific parameters of ERAQSZPs during the diffraction process are shown in Table 1. In addition, it is important to ensure that the focusing characteristics of optics devices are affected by the numerical aperture (NA) in the sagittal direction and the meridian direction:

$$\mathrm{NA} = \sin(\alpha/2), \tag{3}$$

where α is the maximum cone angle of light energy emitted from the zone plate, calculated by Rayleigh criterion, and the resolution is

$$\mathrm{res} = 0.5\lambda/\mathrm{NA}. \tag{4}$$

According to the grating spectral resolution formula, the spectral resolution of ERZPs is affected by the number of zones

$$\lambda/\Delta\lambda = n/2. \tag{5}$$

Theoretically, the greater the number of annular zones in ERZPs, the better the spectral resolution of ERZPs. However, an excessive number of zones will increase the processing difficulty. Meanwhile, there is an upper limit on the number of zones, which satisfies equation[33] $n_{\max} = \Delta t_{\mathrm{pulse}}/\Delta t_{\lambda}$, i.e., its time scale determines the maximum number of zones in the design of ERZPs. When the number of zones is 50, the theoretical spectral resolution can reach 25.

Generally, the paraxial approximation is valid when NA$<$ 0.4 and because the NA of the proposed system in this manuscript is much less than 0.4, the Fresnel diffraction and Kirchhoff diffraction formula can both be applied. However, the Fresnel diffraction formula is a simplified approximation of the Kirchhoff diffraction formula and considering the grazing incidence mode of the reflective device, we perform the

calculation in the manuscript based on the Kirchhoff diffraction formula.

Table 1. Parameters of the ERAQSZPs.

Wavelength λ	41.569 nm
Incident energy E	29.83 eV
Number of bands of zone plate n	50
Object distance R_1	0.75 m
Image distance R_2	1.5 m
Meridian length	42 mm
Sagittal length	3.32 mm
Grazing incidence angle θ	4°
Effective smallest zone width	5.860 μm
NA(meridian) / NA(sagittal)	9.76×10^{-4} / 1.11×10^{-3}

The distribution of complex amplitude $U(P_0)$ behind the diffraction plane can be expressed as

$$U(p_0) = \frac{A}{\mathrm{i}\lambda}\iint_{\Sigma} t(x,z)\frac{\exp[\mathrm{i}k(r_{01}+r_{21})]}{r_{01}r_{21}} \times\frac{[\cos(n,r_{01})-\cos(n,r_{21})]}{2}\mathrm{d}s, \tag{6}$$

where A is a constant, $t(x,z)$ is the reflection of ERAQSZPs, $k=2\pi/\lambda$ represents the wave number, r_{21} is the distance from the light source to a point on the zone plates, and r_{01} is the distance from the observation point to the proposed zone plates. After calculating the complex amplitude, the light intensity distribution $I(P_0)$ can be obtained from $I(P_0)=|U(P_0)|^2$.

Based on Eq. (6), the focusing performance of ERAQSZPs and ERSZPs are presented in Fig. 3 under the same conditions. In detail, figures 3(a) and 3(c) illustrate the images and intensity profiles for the ERSZPs and proposed ERAQSZPs, respectively. Meanwhile, because the ERZPs have a large area, and therefore unavoidably bring a massive amount of computational effort, it is also necessary to approximate and simplify the Kirchhoff diffraction integral formula.

From the comparison in Fig. 3, it can be deduced that both the conventional ERSZPs and proposed ERAQSZPs can generate a circular optical vortex in the image plane. In addition, we also calculated that the ERAQSZPs preserve the same resolution as those of the ERSZPs along the meridian direction and the sagittal direction, which are 21 μm and 19 μm, respectively. According to Eq. (4), the theoretical spatial resolution in the sagittal direction and the meridian direction of ERAQSZPs are 21.27 μm and 18.78 μm, respectively. Compared with the value according to Eq. (4), the deviation is lower to 0.9%, indicating a good agreement between our numerical calculation and theoretical prediction. Moreover, by comparing the ERAQSZPs with a different zone number, say 100, which has a focusing size of 15 μm (FWHM), we have also concluded that the spectral resolution can be significantly improved by optimizing the parameters of the zone plates.

Nevertheless, as we mentioned above, it is known to us that considering the abrupt reflection with that of the conventional binary DOEs, ERZPs and ERSZPs unavoidably act as a multifocal lens, which may suffer from multifocal properties. Namely, the generated OVs beam from the ERSZPs will inevitably superimpose harmonic components whose wavelength is $1/\mathcal{E}$ ($\mathcal{E}=1,2,3,\ldots$) times of the fundamental wave wavelength, which lowers the diffraction efficiency and also increases the background noise. To alleviate these spurious effects originating from the higher foci, ERAQSZPs were proposed to avert the interference of higher-order foci with an ideal sinusoidal reflectance, such as that of ideal GSZPs between the transparent and opaque grooves.

Furthermore, it is noticeable that for conventional ERZPs, to protect the focal spot from the pollution of zeroth diffraction order, a part of the ERZPs has been adopted and the area of the zeroth order diffraction is sufficiently far away from the focal spot. However, in our physical design, to pursue an excellent focusing performance, as well as circular symmetrical phase structure of the OVs, the overall effective area of the ERAQSZPs has been exploited. Typically, in numerical process, we also select the incident beam containing the energy of E and $3E$ for a direct comparison and validation. From Figs. 3(b) and 3(d), we can deduce that apart from the optical vortex imaged by the first primary foci of the ERSZPs, the optical vortex imaged by the third order foci is also overlapped at the same coordinate position. In contrast to the overlapping of the OVs with different higher-order foci, such as those of the ERSZPs, the higher-order foci have been suppressed to lower than three orders of magnitude compared with the intensity of first primacy focus of the ERAQSZPs. This enables it to be an effective alternative to direct a new avenue toward improving the performance of optical image processing, optical capture, x-ray fluorescence spectra, forbidden transition, and so on. Concurrently, we have also calculated the diffraction efficiency of ERSZPs and ERAQSZPs, which are 9.6% and 6%, respectively. Compared with the ERSZPs, although a resultant relative lower transmissive or reflective energy will influence and slightly reduce the diffraction efficiency of the first primacy foci, the ERAQSZPs still exhibit the desired diffraction efficiency which is very close to the value of ideal single-focus GZPs at 6.25%.

Note that to verify the superior performance of the ERAQSZPs as an excellent monochromator, the energy resolution that has to be achieved to separate two adjacent harmonics is also an important factor. To more accurately determine the spectral resolution of ERAQSZPs under Eq. (5), we chose the energy of chromatic light sources to be 29.83 eV and 29.83 ± 1.2 eV (corresponding wavelengths are 41.311 nm, 41.569 nm, and 39.961 nm, respectively). The simulation diagram is shown in Fig. 4, and the three adjacent harmonics can be precisely separated, with a spectral resolution of

$\lambda/\Delta\lambda = 24.86$, which agrees well with the theoretical calculation ($\lambda/\Delta\lambda = n/2 = 25$). With the increase of the number of zone of the ERAQSZPs, its spectral resolution will also be better. In our calculations, the theoretical spectral resolution of ERAQSZPs can reach about 500 when $n = 1000$. Because of the long calculation time, no further simulation has been done. These results pave the way to generate attosecond vortices with controllable OAM.

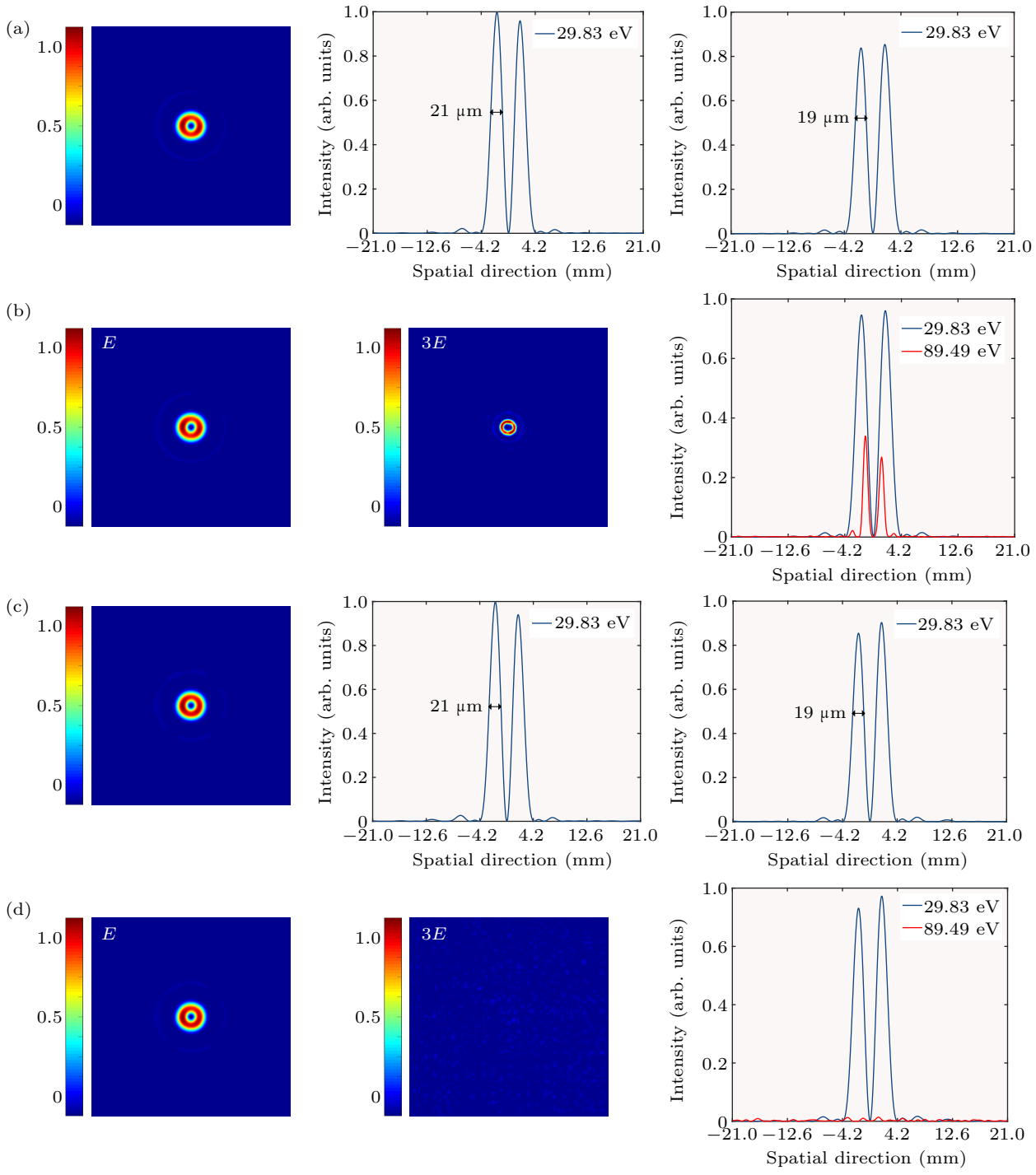


Fig. 3. The intensity distributions on the image plane and the focusing characteristics in the meridian and sagittal directions of ERSZPs (a) and ERAQSZPs (c), respectively, at the design incident intensity of $E = 29.83$ eV; (b) and (d) are the focusing diagram and diffraction intensity peak distribution of ERSZPs and ERAQSZPs at the incident intensity of E and $3E$, respectively.

To accurately determine the focus position and image plane, and enable OVs with different incident energies to be imaged at different positions, based on the grating method,[49] we explore a new approach to perform the calculation.

In the grating method, to calculate its first-order diffraction, we assume that n-band (transparent) and $(n-1)$-band (opaque) are one period of the grating, the period of the grating can be written as

$$d_n = \left(\sqrt{n\lambda} - \sqrt{(n-1)\lambda f}\right)$$

$$+\left(\sqrt{(n-1)\lambda f}-\sqrt{(n-2)\lambda f}\right)$$
$$=\sqrt{\lambda f}\left(\frac{1}{\sqrt{n}+\sqrt{n-1}}+\frac{1}{\sqrt{n-1}+\sqrt{n-2}}\right)$$
$$=\frac{\sqrt{\lambda f}}{\sqrt{n}},\ (n\geq 1). \tag{7}$$

According to Eq. (7), if the number of annular bands is n, the central energy is E_1 (λ_1), and the focusing position corresponding to the central energy is f, then we can calculate the value of the grating period d_n. When the selected energy is E_2 (λ_2), which is different from the central energy, the expression of the focusing position f_2 of E_2 can be obtained by using the grating formula $\sin(\theta)=\lambda/d_n$:

$$f_2=\lambda_1 f_1/\lambda_2. \tag{8}$$

The energy resolution that has to be achieved to separate two adjacent harmonics varies from $E/\Delta E=8.5$ at 26.69 eV (harmonic 17) to $E/\Delta E=11.5$ at 36.11 eV (harmonic 23), considering that two adjacent harmonics have $\Delta E=3.14$ eV separation. Based on the spectral resolution calculated above, EAQSZPs can achieve this energy resolution. During simulation validation, based on the Eqs. (7) and (8), we further confirm and examine the excellent performance of the ERAQSZPs as an effective monochromator by dispersing and focusing the HHG with different harmonic orders. We carry out the verification by employing 19-order (29.83 eV) generated by infrared laser and rare gas Ar as the central energy to explore the corresponding focus positions of 17-order (26.69 eV), 21-order (32.97 eV) and 23-order (36.11 eV). As illustrated in Fig. 5, it is obvious that after modulating by the ERAQSZPs, there are not only sequence circular higher harmonic OVs with different energies can be generated on different image planes but the OVs can also be dispersed and focused on different positions without the interference of higher-order foci by other harmonic orders.

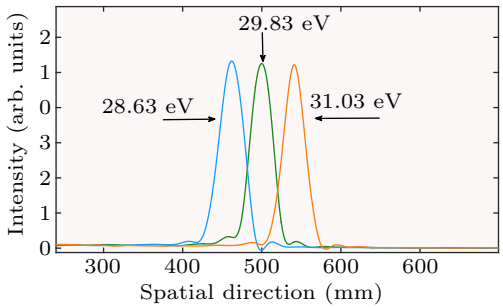


Fig. 4. The distribution diagram of the spectral direction intensity of 28.63 eV, 29.83 eV, and 31.03 eV from left-hand to right-hand.

Additionally, in considering that the optical vortex carrying OAM can transfer energy to other physical objects, the focusing characteristics of ERAQSZPs with different TCs are further investigated. The intensity profiles, vortex distributions, and phase distributions of the focused beams in the first primacy image planes with different TCs of ERAQSZPs are schematically exhibited in Fig. 6. Specifically, considering the optical device with an integer TC gives an isotropic vortical focus, when $P=1$, the vortex beam is characterized by a central dark region, the isosurface presents a helical structure which increases by 2π with each loop around the center of the beam. When $P=2$, the phase increases by 4π for every loop around the center of the vortex beam, indicating that it can be widely used in the fields of isotropic edge enhancement. In addition, the size and radii of the OVs can be increased with the increasing TCs. Nevertheless, the amplitude or phase gradient features in some orientations are more interesting than others. Consequently, anisotropic edge-enhanced imaging technology is required. In particular, in our physical design, the ERAQSZPs can be freely designed with integral and factional TCs. It is apparent from the second column of Fig. 6 that for the case of fractional TCs, the intensity distribution is an uneven screw and the symmetry of the focusing process will be broken down, indicating it to be an effective way to generate orientation-selective anisotropic vortex foci. Importantly, according to our calculation, the performance of the single-order focusing of ERAQSZPs exhibits high stability with negligible fluctuation under different TCs, i.e., maintaining three orders of magnitude suppression ratio. In addition, to further evaluate the quality of laser beams with OAM,[50] we have also calculated the mode purity of the generated OVs with TCs of $P=1$ and $P=2$, which are 69.4% and 62.6%, respectively. These findings imply that the present approach holds promising prospects in practical applications, such as in optical tweezers and optical spanners for particle manipulation.

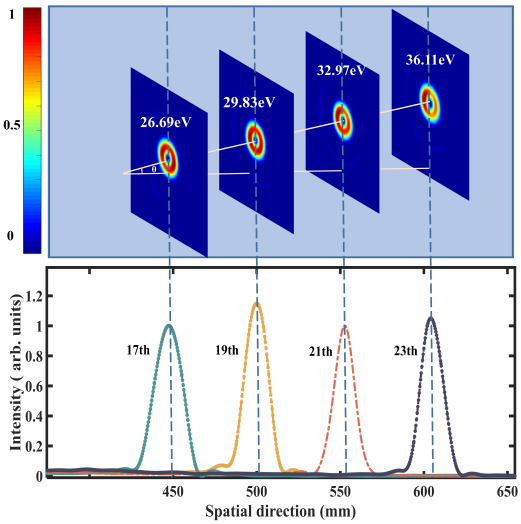


Fig. 5. Focus distribution and spectral direction intensity distribution of different energy wavelengths incident on ERAQSZPs.

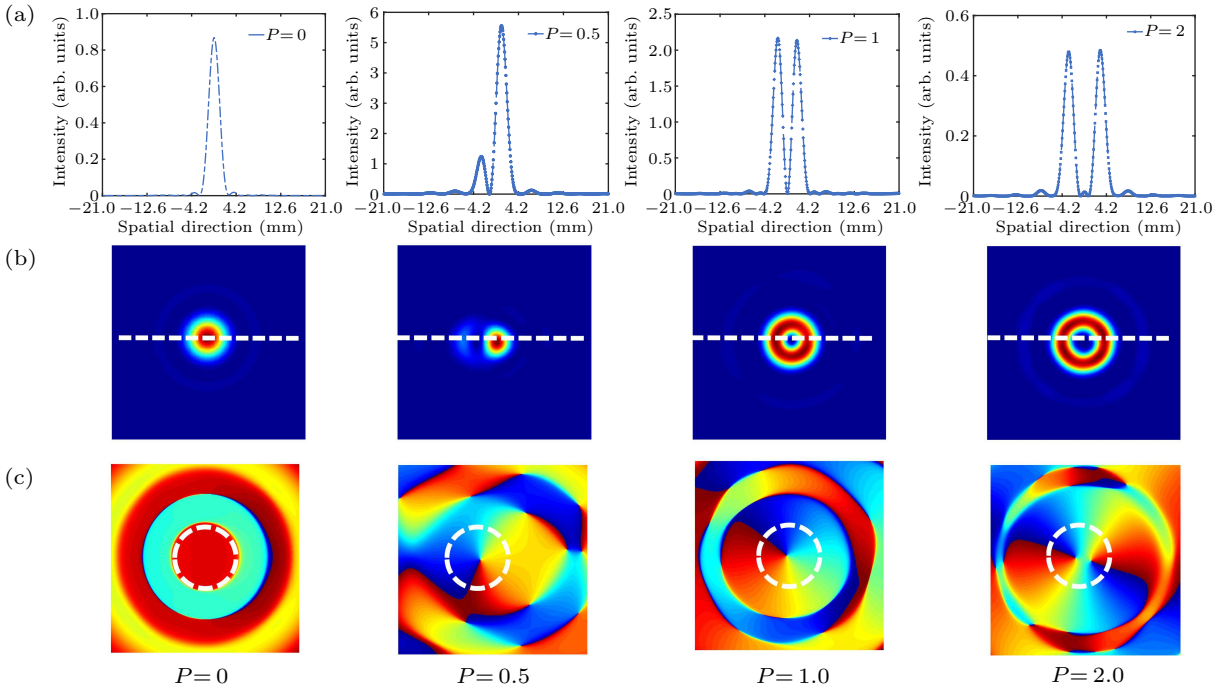


Fig. 6. The intensity profiles (a), vortex distributions (b), and phase distribution (c) of the first primary focus surface of ERAQSZPs with different TCs.

4. Conclusion

In this work, by combining the ERZPs with single-focus SZPs, we have established a methodology that was have termed ERAQSZPs to generate zero axial irradiance without the interference of higher-order foci, from x-rays to extreme ultraviolet regions. In contrast to the abrupt structures (for example) of the ERZPs, the central idea is to realize the desired sinusoidal reflectance by properly arranging a series of randomly distributed annulus quadrangle-shaped nanometer structure apertures. Based on the Fresnel–Kirchhoff diffraction theory and convolution theorem, the focusing performance of the ERAQSZPs has been calculated in detail. Relative to the multi-foci irradiance generated by the ERZPs, our new idea can generate OVs with controllable OAM, and can suppress the unavoidable higher-order foci with a purity and high-resolution spectrum. Typically, according to our physical design, the ERAQSZPs are fabricated on a bulk substrate. Therefore, our new idea can significantly reduce the difficulty in the fabrication process, making it a potential alternative for generating attosecond vortices with controllable OAM. These findings are expected to open a new avenue toward improving the performance of optical image processing, optical capture, x-ray fluorescence spectra, forbidden transition, and so on.

Acknowledgments

Project supported by the National Natural Science Foundation of China (Grant Nos. 12174350, 12275253, and 12275250), the Program of Science and Technology on Plasma Physics Laboratory, China Academy of Engineering Physics (Grant No. 6142A04200107), and the National Natural Science Foundation, Youth Fund (Grant No. 12105268).

References

[1] Shen Y J, Wang X J, Xie Z W, Min C J, Fu X, Liu Q, Gong M L and Yuan X C 2019 *Light Sci. Appl.* **8** 2095
[2] Xia M, Yin Y L, Pei C Y, Ye Y E, Gu R X, Yan K, Wu D, Xia Y and Yin J P 2021 *Chin. Phys. B* **30** 114202
[3] Genevieve G, Jonathan L, Kyung T K, Hammond T J, Frumker E, Boyd R W and Corkum P B 2014 *Phys. Rev. Lett.* **113** 153901
[4] Rego L, Dorney K M, Brooks N J, Nguyen Q L, Liao C T, San R J, Couch D E, Liu A, Pisanty E, Lewenstein M, Plaja L, Kapteyn H C, Murnane M M and Hernandez G C 2019 *Science* **364** 1253
[5] Wang Z, Liu W Z, Zhao M X, Wang J J, Zhang Y W, Chen A, Guan F, Liu X H, Shi L and Zi J 2020 *Nat. Photon.* **14** 623
[6] Zhi S T, Zhang H J and Zhang D X 2012 *Acta Phys. Sin.* **61** 024207 (in Chinese)
[7] Nishiguchi D, Aranson I S, Snezhko A and Sokolov A 2018 *Nat. Commun.* **9** 4486
[8] Pascucci M, Ganesan S, Tripathi A, Katz O, Emiliani V and Guillon M 2019 *Nat. Commun.* **10** 1327
[9] Jesacher A, Fürhapter S, Bernet S and Ritsch-Marte M 2005 *Phys. Rev. Lett.* **94** 233902
[10] Dong M, Zhao C L, Cai Y J and Yang Y J 2021 *Sci. China-Phys. Mech. Astron.* **64** 224201
[11] Bliokh K Y 2021 *Phys. Rev. Lett.* **126** 243601
[12] Dong, L W, Ye F W, Wang J D and Li Y P 2004 *Acta Phys. Sin.* **53** 3353 (in Chinese)
[13] Zhao Z C, Yang X F, Xu T X, He J R, Gong Q X, Du Y L, Dong L, Yuan B and Ma F Y 2018 *Acta Phys. Sin.* **67** 014203 (in Chinese)
[14] Zheng C L, Su S L, Zang H P, Ji Z W, Tian Y Z, Chen S, Mu K J, Wei L, Fan Q P, Wang C K, Zhu X L, Xie C Q, Cao L F and Liang E J 2018 *Appl. Opt.* **57** 802
[15] Chen J, Kuang D F and Fang Z L 2009 *Chin. Phys. Lett.* **26** 094210
[16] Liu Z W, Yan S, Liu H G and Chen X F 2019 *Phys. Rev. Lett.* **123** 183902
[17] Zang H P, Zheng C L, Fan Q P, Wang C K, Wei L, Cao L F, Wang X G and Liang E J 2018 *Chin. Opt. Lett.* **16** 080501
[18] Liu Y J, Dai H T, Sun X W and Huang T J 2019 *Opt. Exp.* **17** 12418
[19] Sakdinawat A and Attwood D 2010 *Nat. Photon.* **4** 840
[20] Fabrizio E D, Romanato F, Gentili M, Cabrini S, Kaulich B, Susini J and Barrett R 1999 *Nature* **401** 895

[21] Zhang Y X, Rykovanov S, Shi M Y, Zhong C L, He X T, Qiao B and Zepf M 2020 *Phys. Rev. Lett.* **124** 114802

[22] Ouyang X, Xu Y, Xian M C, Feng Z W, Zhu L W, Cao Y Y, Lan S, Guan B O, Qiu C W, Gu M and Li X P 2021 *Nat. Photon.* **15** 901

[23] Gaudin J, Rehbein S, Guttmann P, Godé S, Schneider G, Wernet P and Eberhardt W 2008 *J. Appl. Phys.* **104** 033112

[24] Zürch M, Kern C, Hansinger P, Dreischuh A and Spielmann C 2012 *Nat. Phys.* **8** 743

[25] Turpin A, Rego A, Picón A, Román J S and García C H 2017 *Sci. Rep.* **7** 43888

[26] Dorney K M, Rego L, Brooks N J, Román J S, Liao C T, Ellis J L, Zusin D, Gentry C, Nguyen Q L, Shaw J M, Picón A, Plaja L, Kapteyn H C, Murnane M M and García C H 2019 *Nat. Photon.* **13** 123

[27] Wei L, Gao Y L, Wen X L, Zhao Z Q, Cao L F and Gu Y Q 2013 *J. Opt. Soc. Am. A* **30** 233

[28] Schneider G 1997 *Appl. Phys. Lett.* **71** 2242

[29] Michette A G, Pfauntsch S J, Erko A, Firsov A and Svintsov A 2005 *Opt. Commun.* **245** 249

[30] Yang Z H, Zhao Z Q, Wei L, Zhang Q Q, Qian F, Gu Y Q and Lei L F 2014 *Chin. Phys. Lett.* **31** 050701

[31] Xie C Q, Zhu X L, Shi L N and Liu M 2010 *Opt. Lett.* **35** 1765

[32] Fan Q P, Wang S Y, Yang Z H, Wei L, Hu F, Zang H P, Zhang Q Q, Wang C K, Jiang G and Cao L F 2017 *J. Modern Opt.* **64** 244

[33] Gao N, Xie C Q, Li C, Jin C S and Liu M 2011 *Appl. Phys. Lett.* **98** 151106

[34] Ghadimi Nassiri M and Brasselet E 2018 *Phys. Rev. Lett.* **121** 213901

[35] Xie C Q, Zhu X L, Li H L, Shi L N, Hua Y L and Liu M 2012 *Opt. Lett.* **37** 749

[36] Zang H P, Zheng C L, Ji Z W, Fan Q P, Wei L, Li Y J, Mu K J, Chen S, WangC K, Zhu X L, Xie C Q, Cao L F, Liang E J 2019 *Chin. Phys. B* **28** 064201

[37] Xie C Q, Zhu X L, Li H L, Shi L N and Wang Y H 2010 *Opt. Lett.* **35** 4048

[38] Shu J H, Chen Z Y, Pu J X and Liu Y X 2011 *Chin. Phys. B* **20** 114202

[39] Zang H P, Wang C K, Gao Y L, Zhou W M, Kuang L Y, Wei L, Fan W, Zhang W H, Zhao Z Q, Cao L F, Gu Y Q, Zhang B H, Jiang G, Zhu X L, Xie C Q, Zhao Y D and Cui M Q 2012 *Appl. Phys. Lett.* **100** 111904

[40] Wei L, Kuang L Y, Fan W, Zang H P, Cao L F, Gu Y Y and Wang X F 2011 *Opt. Exp.* **19** 21419

[41] Suzuki Y S, Takeuchi A, Takano H, Kentaro U, Toshihiko Q and Katsuaki I 2004 *Rev. Sci. Instrum.* **75** 1155

[42] Chen Y, Wei L, Zhang Q Q, Fan Q P, Yang Z H and Cao L F 2020 *Chin. Phys. B* **29** 104202

[43] Erko A, Firsov A and Senf F 2012 *SpectroChim. Acta Part. B: At. Spectrosc.* **67** 57

[44] Zang H P, Miao Z L, Wang M G, Fan Q P, Wei L, Wang C K, Zhou W M, Hua Y L, Cao L F, Xue X L and Guo H Z 2022 *Sci. China-Phys. Mech. Astron.* **65** 294212

[45] Ran L L, Guo Z Y, Qu S L 2012 *Chin. Phys. B* **21** 104206

[46] Patchkovskii S and Spanner M 2012 *Nat. Phys.* **8** 707

[47] Zhang Y X, Yuan J H, Qu Y W, Zhou X, Yan B B, Wu Q, Wang K R, Sang X Z, Long K P and Yu C X 2020 *Chin. Phys. B* **29** 034208

[48] Picón A, Benseny A, Mompart J, Vázquez de Aldana J R, Plaja L, CalvoG F and Roso L 2010 *New J. Phys.* **12** 083053

[49] Attwood D T 1999 *Soft X-Rays and Extreme Ultraviolet Radiation: Principles and Applications* (Cambridge: Cambridge university Press) pp. 329–388

[50] Zhang H, Zeng J, Lu X Y, Wang Z Y, Zhao C L and Cai Y J 2022 *Nanophotonics* **11** 241